Nd—Nd Bond in I_h and D_{5h} Cage Isomers of $Nd_2@C_{80}$ Stabilized by Electrophilic CF_3 Addition

Wei Yang, Georgios Velkos, Marco Rosenkranz, Sandra Schiemenz, Fupin Liu,* and Alexey A. Popov*

Synthesis of molecular compounds with metal–metal bonds between 4f elements is recognized as one of the fascinating milestones in lanthanide metallochemistry. The main focus of such studies is on heavy lanthanides due to the interest in their magnetism, while bonding between light lanthanides remains unexplored. In this work, the Nd—Nd bonding in Nd-dimetallofullerenes as a case study of metal–metal bonding between early lanthanides is demonstrated. Combined experimental and computational study proves that pristine $Nd_2@C_{80}$ has an open shell structure with a single electron occupying the Nd—Nd bonding orbital. $Nd_2@C_{80}$ is stabilized by a one-electron reduction and further by the electrophilic CF_3 addition to $[Nd_2@C_{80}]^-$. Single-crystal X-ray diffraction reveals the formation of two $Nd_2@C_{80}(CF_3)$ isomers with D_{5h}-C_{80} and I_h-C_{80} carbon cages, both featuring a single-electron Nd—Nd bond with the length of 3.78–3.79 Å. The mutual influence of the exohedral CF_3 group and endohedral metal dimer in determining the molecular structure of the adducts is analyzed. Unlike Tb or Dy analogs, which are strong single-molecule magnets with high blocking temperature of magnetization, the slow relaxation of magnetization in $Nd_2@I_h$-$C_{80}(CF_3)$ is detectable via out-of-phase magnetic susceptibility only below 3 K and in the presence of magnetic field.

1. Introduction

Stabilization of unconventional metallic species and thereby a broadening of the metallochemistry frontiers is one of the unique features of endohedral metallofullerenes (EMFs).[1] A spectacular example of this sort is the realization of the lanthanide–lanthanide bonding within the fullerene cage,[2] which for a long time deemed not possible in conventional lanthanide chemistry. $M_2@C_{79}N$ (M = Y, Tb, Gd) azafullerenes with single-electron

W. Yang, G. Velkos, M. Rosenkranz, S. Schiemenz, F. Liu, A. A. Popov
Leibniz Institute for Solid State and Materials Research
Helmholtzstraße 20, 01069 Dresden, Germany
E-mail: f.liu@ifw-dresden.de; a.popov@ifw-dresden.de

metal–metal bonds were discovered in 2008–2011.[3] In parallel, an understanding that two-electron metal–metal bonds are quite ubiquitous for dimetallofullerenes (di-EMFs) of Lu, Er, and Y was developed in a series of experimental and computational studies.[2,4] Single-electron lanthanide–lanthanide bonds were also stabilized in a series of $M_2@C_{80}R$ derivatives (R = CH_2Ph, CF_3).[5] Three-center metal–metal bonding was suggested first in trimetallofullerenes $M_3@C_{2n}$ based mainly on computational studies,[6] and was then found experimentally in carbide clusterfullerenes $M_3C_2@C_{80}$ (M = Dy, Er).[7] Single-electron bonds in $M_2@C_{79}N$ and $M_2@C_{80}R$ are especially interesting as the way to create very strong magnetic interactions between 4f magnetic moments,[3,5,8,9] leading to high-performance single molecule magnets.[5,10] The first non-fullerene complexes with two and three-center single electron bonds between lanthanides were also obtained recently.[11]

Formation of M—M bonds in di-EMFs is achieved by the guest-to-host electron transfer as schematically shown in **Figure 1a**. Some fullerene cages, such as I_h-C_{80}, are efficient acceptors of six electrons, and when dimers of early lanthanides La and Ce are encapsulated within, they readily transfer all six valence electrons to the fullerene host. The $La_2@C_{80}$ molecule has the singlet (S) ground state, and no La—La bond is present. For heavier lanthanides, such as Gd and beyond, the metal dimer orbitals have lower energies, and only five electrons are transferred to the fullerene. $M_2@C_{80}$ molecules with such metals feature a single-electron M—M bond, while the carbon cage has an open-shell electronic structure with one "missing" electron. For Y and heavy lanthanides, this pseudo-triplet electronic state (denoted as pT hereafter) is lower in energy than the pseudo-singlet (pS) with six-electron transfer (we use prefix "pseudo" to underline that spins of 4f electrons are not considered and thus the true spin multiplicity of the molecule can be different).[5f,12] The switch between pS and pT ground states occurs somewhere between Ce and Gd, but di-EMFs of light lanthanides other than La and Ce are not well studied. Sm and Eu prefer divalent state in EMFs, and reported Sm di-EMFs do not feature Sm—Sm bonds.[13] Pr and Nd adopt the Ln^{III} state in mono-EMFs, but not much is known about their di-EMFs so far. An early report

ADVANCED
SCIENCE NEWS
www.advancedsciencenews.com

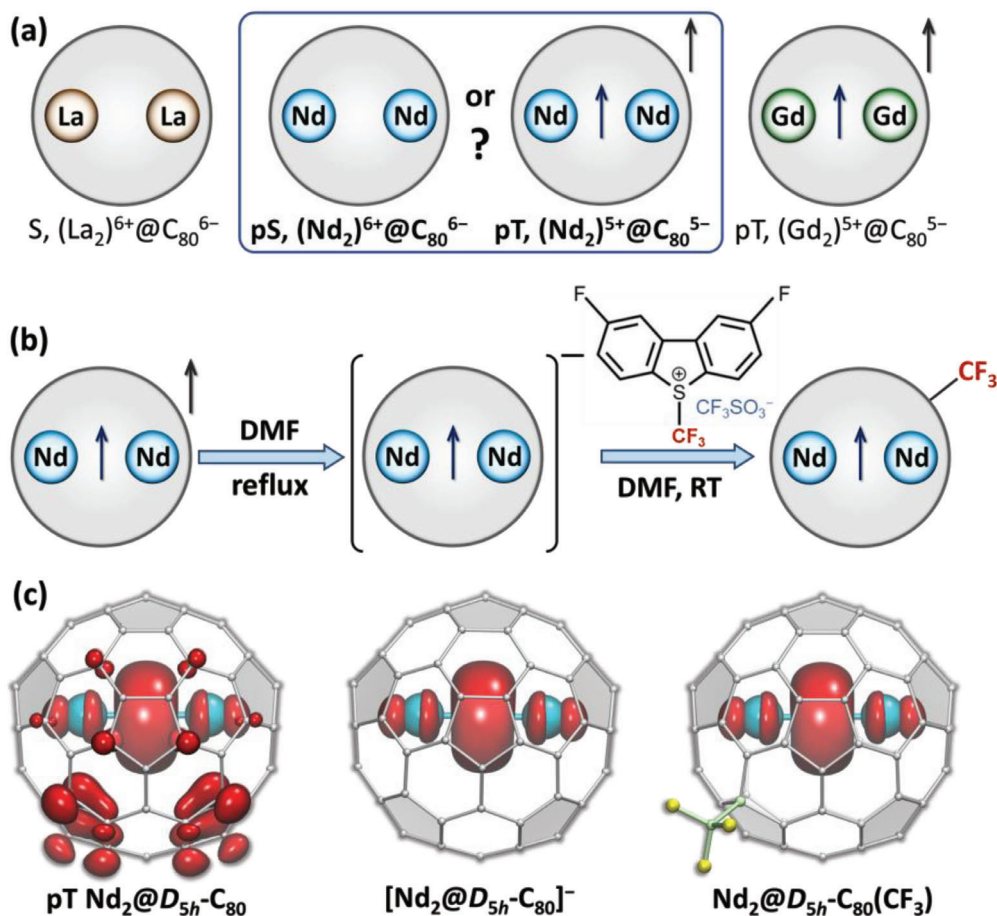ADVANCED
SCIENCE
Open Access
www.advancedscience.com

Figure 1. a) Schematic description of the ground-state electronic structure of dimetallofullerenes $M_2@C_{80}$: singlet (S) $La_2@C_{80}$ with trivalent La, pseudo-triplet (pT) $Gd_2@C_{80}$ with $(Gd_2)^{5+}$ dimer and an open-shell structure of the fullerene, and the two corresponding possibilities for $Nd_2@C_{80}$. b) Schematic description of the extraction of $Nd_2@C_{80}$ (along with other EMFs) by hot DMF in the form of $[Nd_2@C_{80}]^-$ anion, followed by the reaction with Umemoto reagent II with formation of the $Nd_2@C_{80}(CF_3)$ adduct. c) DFT-computed valence spin density distribution in $Nd_2@D_{5h}-C_{80}$ (pseudo-triplet), $[Nd_2@D_{5h}-C_{80}]^-$ anion, and $Nd_2@D_{5h}-C_{80}(CF_3)$. Similar spin density distributions are obtained for the I_h-C_{80} cage isomer (Figure S2, Supporting Information).

showed that $Pr_2@C_{80}$ can be extracted from the EMF soot and proved the Pr^{III} state by XPS technique,[14] whereas more recent studies addressed the structure and properties of $Pr_2@C_{72}$.[15] To the best of our knowledge, there are no reports on Nd-based di-EMFs at all, in contrast to the relatively well studied mono-EMF $Nd@C_{82}$.[16]

In this work, we aim at the understanding of the metal–metal bonding in light lanthanides and focus on Nd as the lanthanide with the least studied di-EMFs. We demonstrate that while neutral $Nd_2@C_{80}$ is non-accessible for the analysis in the pristine state, it can be stabilized as an anion and in the form of CF_3 mono-adduct. Two isomers of $Nd_2@C_{80}(CF_3)$ with D_{5h} and I_h cage symmetry are characterized by single-crystal X-ray diffraction, proving the ability of Nd to form single-electron Nd—Nd bonds. The factors affecting regioselectivity of electrophilic CF_3 addition to EMF anions are analyzed. Magnetic properties of $Nd_2@C_{80}(CF_3)$ are studied by SQUID (superconducting quantum interference device) magnetometry to understand if the single-electron Nd—Nd bond leads to the single-molecule magnetism.

2. Results and Discussion

2.1. Electronic Structure of $M_2@C_{80}$

Metallofullerenes are normally obtained by arc-discharge evaporation of graphite followed by solvent extraction from the soot, but their solubility depends on the electronic state. Those with the closed-shell electronic structure are usually soluble in CS_2 and aromatic solvents. Open-shell EMFs show low to negligible solubility in CS_2 and mainly remain in the soot after CS_2 extraction because of polymerization or interaction with soot particles. However, low-gap and open-shell fullerenes can be dissolved in boiling dimethylformamide (DMF), which is a poor solvent for empty fullerenes.[17] During the DMF extraction, such fullerenes are reduced and extracted in the form of anions, which are well-soluble in polar DMF (Figure 1b),[18] unlike the closed-shell fullerenes with large HOMO–LUMO gap, which remain neutral and hence poorly soluble in DMF (HOMO and LUMO refer to highest-occupied and lowest-unoccupied molecular orbitals). Particularly for $M_2@C_{80}$ di-EMFs, the extraction with CS_2
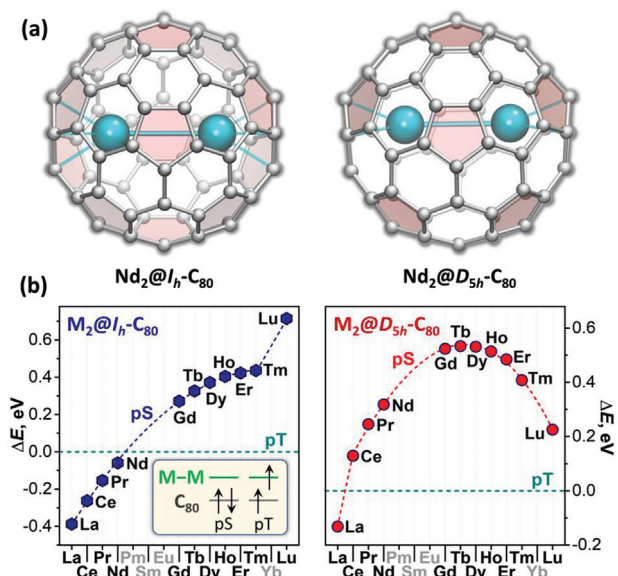
Figure 2. a) Molecular structure of $Nd_2@C_{80}$ isomers with I_h and D_{5h} cage symmetry. Both molecules are shown along the C_5 axis of the carbon cage; pentagons are shaded to highlight different relative orientations of upper and lower hemispheres in I_h and D_{5h} isomers. b) Relative energies of pseudo-singlet (pS) state of $M_2@C_{80}$ molecules versus pseudo-triplet (pT) states as predicted by DFT calculations at the PBE0//PBE level (I_h-C_{80} isomer—left, D_{5h}-C_{80} isomer—right). Four lanthanides were not considered in calculations, because Pm is not available for experimental work, while Sm, Eu, and Yb adopt 2+ oxidation state in EMFs.

and DMF gives the first indication on the electronic structure. While singlet La and Ce di-EMFs are soluble in CS_2, pseudo-triplet $M_2@C_{80}$ di-EMFs of heavy lanthanides starting from Gd can be only extracted by DMF.[5,19]

To identify a transition point between the two types, we first perform a systematic DFT (density functional theory) study of $M_2@C_{80}$ molecules in pS and pT states for the whole lanthanide row using two fullerene isomers with I_h and D_{5h} cage symmetry (**Figure 2**). Calculations showed that in the $M_2@I_h$-C_{80} series, the pT state is gradually stabilized with the growth of the atomic number (Figure 2b and Table S1a, Supporting Information). The pS state is more stable for La–Nd, whereas the pT state is more preferable from Gd to Lu. In the $M_2@D_{5h}$-C_{80} series, the fullerene-based HOMO has higher energy than in I_h isomers, and the pT state is predicted to be more stable for all lanthanides except for La. However, as the M—M bonding MO gets stabilized along the lanthanide row, its energy gap to the fullerene-based HOMO becomes very small, and the orbitals start mixing (Figure S1, Supporting Information). For pS-$Lu_2@C_{80}$, the occupied orbital becomes of the dominant Lu—Lu bonding nature, whereas the LUMO acquires a fullerene-based character. This orbital quasi-degeneracy implies a multiconfigurational electronic state and may be problematic for DFT. Nevertheless, the general trend of the gradual stabilization of pT along the lanthanide row holds and qualitatively agrees with experimental observations, although the numerical values may be not very accurate.

In the $M_2@I_h$-C_{80} series, Nd is particular close to the transition between the two types of behavior and therefore appears to be an interesting target for the synthesis. DFT PBE0//PBE cal-

culations predict that pS and pT states of $Nd_2@I_h$-C_{80} are nearly degenerate, the former being 0.06 eV more stable (see Table S1b, Supporting Information, for calculations with other DFT functionals). In the closed-shell pS state, the HOMO is localized on the fullerene whereas the LUMO is the Nd—Nd bonding orbital. In the pT state, one electron from the fullerene orbital is promoted to the Nd—Nd bonding orbital (see inset in Figure 2b). The valence spin density in pT-$Nd_2@C_{80}$ is thus localized both on the Nd—Nd bonding MO and on the fullerene cage (Figure 1c and Figure S2, Supporting Information).

2.2. Synthesis of $Nd_2@C_{80}$

The soot containing Nd-EMFs was obtained by arc-discharge evaporation of graphite rods filled with a mixture of Nd_2O_3 and graphite powders under helium atmosphere (180 mbar). Extraction behavior of Nd di-EMFs appeared similar to those of heavy lanthanides. We could not detect $Nd_2@C_{80}$ in mass-spectra of CS_2 extracts, but its signal was readily observed in mass-spectra after extraction with DMF (Figures S3 and S4, Supporting Information). Furthermore, our attempts to obtain neutral $Nd_2@C_{80}$ by a treatment of the anionic Nd-EMF extract with $CHCl_2COOH$ in acetone could only recover neutral $Nd@C_{82}$. For comparison, an analogous reaction with La-EMF anions produced both $La@C_{82}$ and $La_2@C_{80}$.[20] Thus, we conclude that $Nd_2@C_{80}$ is not stable in the neutral form, suggesting its pT ground state. This open-shell electronic structure is responsible for the low solubility of neutral $Nd_2@C_{80}$ and its facile reduction to a monoanionic state. In the $[Nd_2@C_{80}]^-$ anion, the fullerene cage attains a closed-shell electronic configuration, while the Nd—Nd bonding orbital still hosts an unpaired electron (Figure 1c and Figure S2, Supporting Information). Interestingly, CS_2 extraction of Pr-EMFs obtained in a similar arc-discharge procedure did produce $Pr_2@C_{2n}$ species detectable in mass-spectra (Figure S3, Supporting Information), in line with the earlier report on the isolation of $Pr_2@C_{80}$.[14] These results demonstrate that the transition from the pS to the pT ground state of $M_2@C_{80}$ occurs between Pr and Nd.

2.3. Electrophilic Trifluoromethylation of $[Nd_2@C_{80}]^-$

To stabilize $Nd_2@C_{80}$ in the form of a neutral compound, electrophilic trifluoromethylation with 2,8-difluoro-S-(trifluoromethyl)dibenzothiophenium trifluoromethanesulfonate (Umemoto reagent II,[21] URII) was performed. The reaction can be formally described as a $[CF_3]^+$ cation addition to $[EMF]^-$ anions, giving neutral $EMF(CF_3)$ adducts (Figure 1b). We recently found that at the first stage, the reaction of Tb-EMFs with URII exhibited enhanced selectivity to $[Tb_2@I_h$-$C_{80}]^-$.[5] Likewise, optimization of the URII amount in the reaction with Nd-EMF extract in DMF allowed to obtain $Nd_2@C_{80}(CF_3)$ in this work (Figure S5, Supporting Information). When optimized reagent ratio is used, HPLC (high-performance liquid chromatography) profile of the crude reaction product mixture has a dominant fraction in the retention time range of $EMF(CF_3)$ monoadducts (F-I in **Figure 3a**), which mainly contains $Nd_2@C_{80}(CF_3)$. The presence of $Nd_2@C_{80}(CF_3)$, identified
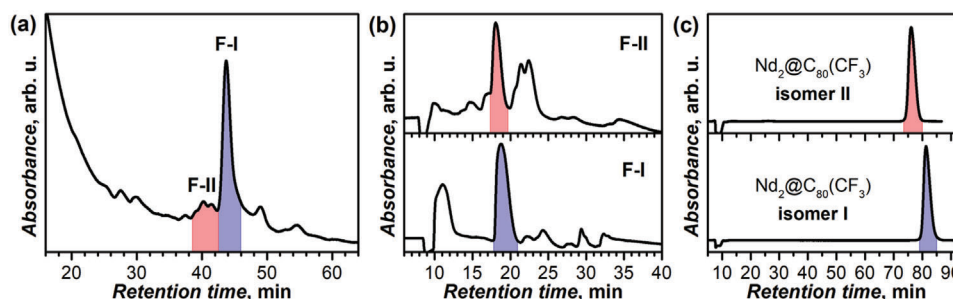
Figure 3. a) HPLC chromatogram of the crude product mixture after reaction of Nd-metallofullerene DMF extract with Umemoto reagent II (linear combination of two Buckyprep columns, toluene, 5 mL min^{-1}); the fractions highlighted by color and denoted as F-I and F-II contain isomers of Nd$_2$@C$_{80}$(CF$_3$) and are separated further; b) The second step separation of fractions F-I and F-II on a Buckyprep-D column (toluene, 2 mL min^{-1}), fractions with Nd$_2$@C$_{80}$(CF$_3$) isomers are highlighted by color. c) HPLC chromatograms of purified Nd$_2$@C$_{80}$(CF$_3$) isomers (Buckyprep column, toluene, 2 mL min^{-1}). Note that the separation of isomer II required an additional HPLC step to remove minor impurity as described in Figure S6, Supporting Information.

as a different isomer, was also found by mass-spectrometry in the preceding fraction (F-II in Figure 3a). Both fractions were then subjected to the second HPLC step with a different column, which gave pure isomer I and almost pure isomer II (Figure 3b). For the latter, an additional step was required to remove some minor admixtures (Figure S6, Supporting Information). The isolated isomers of Nd$_2$@C$_{80}$(CF$_3$) were then characterized by matrix-assisted laser desorption/ionization mass-spectrometry (Figure S7, Supporting Information) and a variety of spectroscopic techniques (**Figure 4**; Figures S8 and S9, Supporting Information). To accumulate sufficient amount of material, 40 arc-discharge evaporations were performed, consuming 68 g of Nd$_2$O$_3$ and yielding eventually 2.5 mg of the major Nd$_2$@C$_{80}$(CF$_3$) isomer. Perfluoroalkylfullerenes usually bear even number of addends,[22] and the odd number of CF$_3$ groups in Nd$_2$@C$_{80}$(CF$_3$) indicates that these adducts have metal-based open-shell character. Indeed, DFT calculations discussed in detail below demonstrate the presence of a single-electron Nd—Nd bond in Nd$_2$@C$_{80}$(CF$_3$) (Figure 1c and Figure S2, Supporting Information).

^{19}F NMR (nuclear magnetic resonance) spectra of each Nd$_2$@C$_{80}$(CF$_3$) isomer at 298 K have only one signal at −78.65 (I) and −78.05 ppm (II), proving their isomeric purity (Figure 4a). Both isomers exhibit considerable temperature dependence of their ^{19}F chemical shifts caused by the magnetic influence

of endohedral Nd$_2$ dimers on the ^{19}F nuclear spins of CF$_3$ groups. However, the paramagnetic shift of Nd$_2$@C$_{80}$(CF$_3$) is much weaker than in Tb$_2$@I$_h$-C$_{80}$(CF$_3$), which exhibits $\delta(^{19}$F) of −251 ppm at 298 K.[5] Note that a conservative estimation of the diamagnetic shift based on the T^{-2} dependence of $\delta(^{19}$F) gives the values near −70 ppm. Carbon chemical shifts in ^{13}C NMR spectra of isomer I (**Figure 5**) were found in the range of 30–190 ppm, some of them with considerable temperature dependence. The number of detectable signals, around 40, is consistent with C_s effective symmetry of the adduct.

Vis-NIR (visible-near infrared) absorption spectra of two isomers are distinctly different (Figure 4b). That of the main isomer I resembles the spectra of Tb$_2$@I$_h$-C$_{80}$(CF$_3$)[5] and M$_2$@I$_h$-C$_{80}$(CH$_2$Ph),[5] whereas the absorption pattern of isomer II is similar to the spectrum of La$_2$@D$_{5h}$-C$_{80}$(C$_3$N$_3$-Ph$_2$).[5] Given that absorption spectra of EMFs and their derivatives are usually weakly influenced by their endohedral species and exohedral groups but are chiefly determined by the fullerene π-system topology, the fullerene cage isomers I$_h$-C$_{80}$ and D$_{5h}$-C$_{80}$ can be assigned to Nd$_2$@C$_{80}$(CF$_3$) isomers I and II, respectively.

The structural conjecture is further corroborated by vibrational spectroscopy. Infrared spectrum of Nd$_2$@C$_{80}$(CF$_3$)-I is virtually identical to the spectrum of Tb$_2$@I$_h$-C$_{80}$(CF$_3$) from ref. [5e] (Figure S8, Supporting Information), both in the position and relative intensity of strong CF$_3$-related modes at 946,
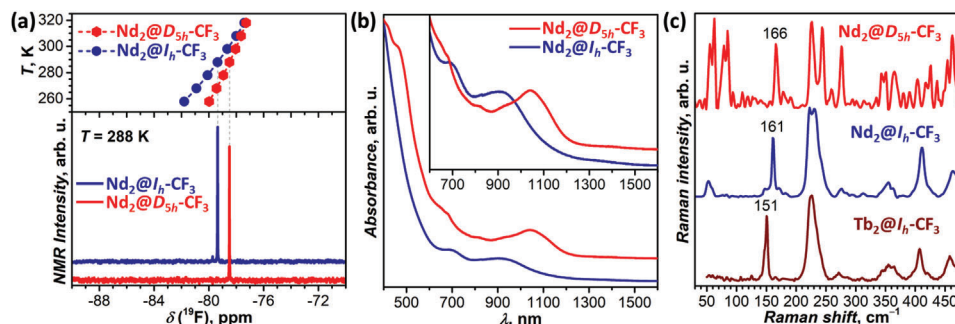

Figure 4. a) ^{19}F NMR spectra of two Nd$_2$@C$_{80}$(CF$_3$) isomers in CS$_2$ solution at 288 K, and the temperature dependence of ^{19}F chemical shifts between 258 and 318 K. b) Vis-NIR absorption spectra of two Nd$_2$@C$_{80}$(CF$_3$) isomers in toluene solution. c) Raman spectra of two Nd$_2$@C$_{80}$(CF$_3$) isomers compared to the spectrum of Tb$_2$@I$_h$-C$_{80}$(CF$_3$) (T = 78 K, excitation at 532 nm).

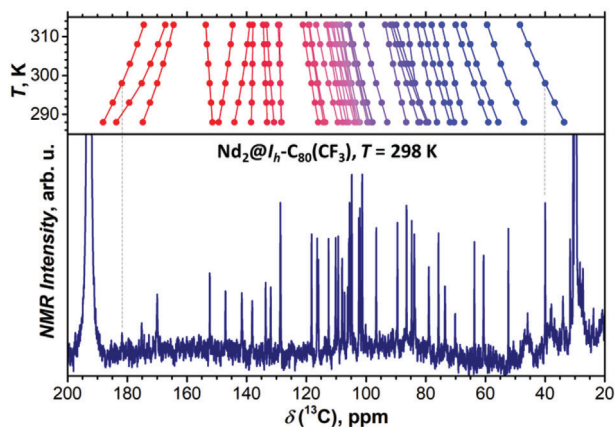**Figure 5.** ^{13}C NMR spectrum of $Nd_2@I_h$-$C_{80}(CF_3)$ in CS_2 measured at 298 K (lower panel) and temperature dependence of chemical shifts assigned to the fullerene carbons (upper panel).

1174–1196, and 1222 cm^{-1}, and in the absorption pattern of weaker cage-based vibration, which suggests that the two compounds are isostructural. Strong CF_3 absorption features in the spectrum of $Nd_2@C_{80}(CF_3)$-II are found at similar positions (943, 1174–1196, and 1237 cm^{-1}) as in $Nd_2@C_{80}(CF_3)$-I, but the spectra are quite different in the range of the fullerene cage modes. Likewise, Raman spectra of $Nd_2@C_{80}(CF_3)$-I and $Tb_2@I_h$-$C_{80}(CF_3)$ are very similar above 200 cm^{-1} (Figure S9, Supporting Information), but are distinct at lower frequencies, where metal-based modes occur (Figure 4c). Particular characteristic is the metal-cage stretching mode, which in lanthanide dimetallofullerenes usually occurs at 140–170 cm^{-1}, has medium-strong Raman intensity and a narrow linewidth. For instance, in $La_2@C_{80}$ it occurs at 163 cm^{-1},[23] in $Gd_2@C_{79}N$ it was found at 156 cm^{-1},[3] while in the $M_2@C_{80}(CH_2Ph)$ series the position varies from 151 cm^{-1} for Gd to 144 cm^{-1} for Er.[5] In $Nd_2@C_{80}(CF_3)$-I this mode occurs at 161 cm^{-1}, comparable to $La_2@C_{80}$, as Nd is relatively light. In $Tb_2@I_h$-$C_{80}(CF_3)$ this vibration is shifted to 151 cm^{-1} owing to the larger mass of Tb. The metal-based mode of $Nd_2@C_{80}(CF_3)$-II occurs at somewhat higher frequency (166 cm^{-1}) than in the isomer I, while vibrational pattern of the fullerene cage is again quite different.

2.4. Crystallographic Analysis

An unambiguous elucidation of molecular structures was obtained by single-crystal X-ray diffraction (SC-XRD) (**Figure 6**). $Nd_2@C_{80}(CF_3)$ in toluene (isomer I) or CS_2 (isomer II) was co-crystallized with nickel octaethylporphyrin (NiOEP) in benzene. X-ray diffraction data collection was carried out at 100 K at the BESSY storage ring (BL14.2, Berlin-Adlershof, Germany).[24] XD-SAPP2.0 suite was employed for data processing.[25] The structure was solved by direct methods and refined by SHELXL-2018.[26] Hydrogen atoms were added geometrically and refined with a riding model. The crystal data are presented in Table S2 (Supporting Information).

The isomer $Nd_2@C_{80}(CF_3)$-I features $I_h(7)$-C_{80} carbon cage and forms monoclinic crystals (C2/c space group) with the composition of $2Nd_2@I_h$-$C_{80}(CF_3)\cdot4NiOEP\cdot1.63C_7H_8\cdot0.37C_6H_6$,
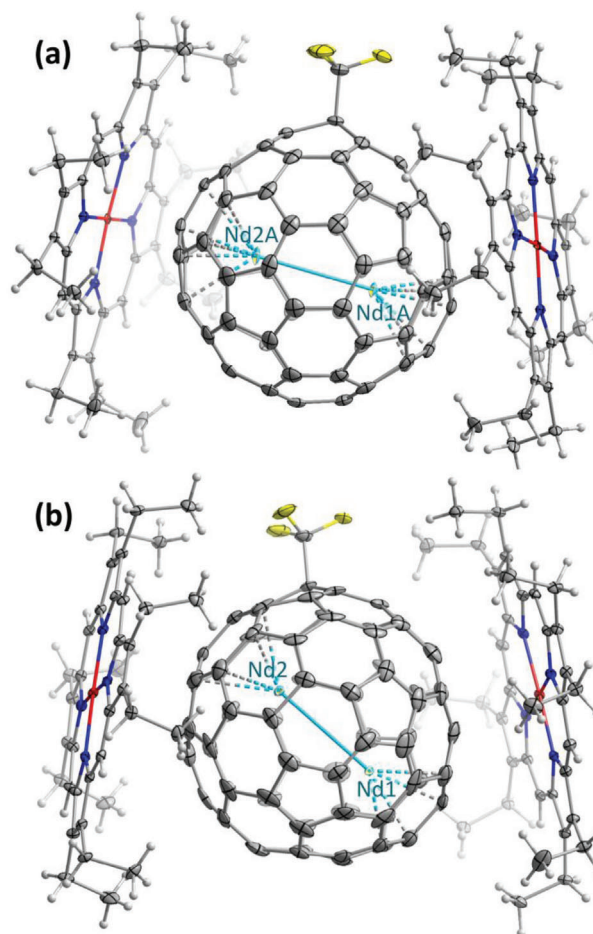
Figure 6. Molecular structures of a) isomer I, $Nd_2@I_h$-$C_{80}(CF_3)$, and b) isomer II, $Nd_2@D_{5h}$-$C_{80}(CF_3)$, in co-crystals with NiOEP. Only single $Nd_2@C_{80}(CF_3)$ moiety with the main Nd sites and two clamping NiOEP molecules are shown for each co-crystal, see Supporting Information for further details. Nd site occupancies are 0.72/0.72 for Nd1A and Nd2A in (a), and 0.22/0.26 (out of 0.5) for Nd1/Nd2 in (b). The displacement parameters are shown at the 30% probability level. Color code: grey for carbon, cyan for Nd, yellow for F, blue for N, white for H, and red for Ni.

closely resembling the crystal structure of $Tb_2@I_h$-$C_{80}(CF_3)$.[5e] The asymmetric unit contains four intact NiOEP molecules exhibiting some degree of translational disorder, one ordered $Nd_2@I_h$-$C_{80}(CF_3)$ molecule (site A), four halves of fullerene molecules statistically disordered over two orientations with half occupancies (sites B and C), and disordered benzene/toluene molecules. Four halves of disordered fullerene molecules are correlated by the C_2 axis of the crystal passing through the molecule (roughly parallel to the C_{80}—CF_3 bond). The Nd_2 dimer is disordered over three positions with occupancies of 0.72, 0.20, and 0.07 in the site A, and over two positions with occupancies of 0.36 and 0.14 in each of the sites B and C (**Figure 7** and Figure S10, Supporting Information). The Nd—Nd bond lengths determined for the major Nd_2 sites are 3.792(2), 3.791(2), and 3.778(2) Å in molecules A, B, and C, respectively. In all the major Nd_2 sites, Nd atoms coordinate fullerene hexagons in η^6-manner, with the shortest Nd—C distances of 2.39–2.44 Å.
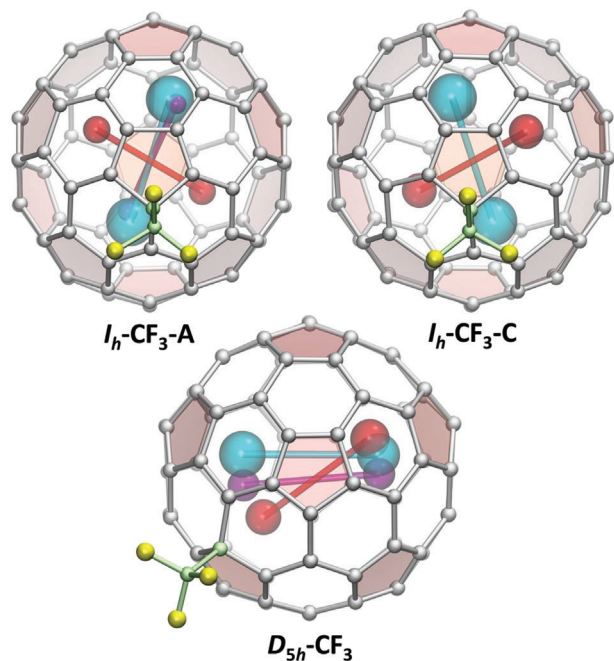
**ADVANCED
SCIENCE NEWS**

www.advancedsciencenews.com

**ADVANCED
SCIENCE**
Open Access

www.advancedscience.com

Figure 7. SC-XRD molecular structures of $Nd_2@C_{80}(CF_3)$ isomers showing disorder of Nd positions. I_h-CF$_3$-A: molecule A of $Nd_2@I_h$-$C_{80}(CF_3)$, Nd_2 sites are cyan (Nd_1A/Nd_2A, 2 × 0.72), red (Nd_3A/Nd_2A, 2 × 0.20), and purple (Nd_5A/Nd_6A, 2 × 0.07). I_h-CF$_3$-C: molecule C of $Nd_2@I_h$-$C_{80}(CF_3)$, Nd_2 sites are cyan (Nd_1C/Nd_2C, 2 × 0.36) and red (Nd_3C/Nd_4C, 2 × 0.14), overlapping fullerene molecule and symmetry related Nd sites are not shown. D_{5h}-CF$_3$: $Nd_2@D_{5h}$-$C_{80}(CF_3)$, Nd_2 sites are cyan (Nd_1/Nd_2, 0.21/0.26), red (Nd_3/Nd_4, 0.17/0.15), and purple (Nd_5/Nd_6, 0.11/0.09), overlapping fullerene molecule and symmetry related Nd sites are not shown. The volume of spheres representing metal atoms scales as their relative occupancy.

The isomer $Nd_2@C_{80}(CF_3)$-II has $D_{5h}(6)$-C_{80} carbon cage and forms co-crystals with the $Nd_2@D_{5h}$-$C_{80}(CF_3)·2NiOEP·C_6H_6$ composition and C2/c space group. The asymmetric unit contains one intact NiOEP molecule, two halves of fullerene molecules with half occupancy correlated by the crystallographic C_2 axis passing through the fullerene molecules, and one intact benzene molecule. The Nd_2 dimer is disordered over three positions (Figure 7) and their symmetry replica, the Nd—Nd bond lengths being 3.788(2) Å for Nd1–Nd2 (occupancy 0.21/0.26), 3.780(3) Å for Nd3–Nd4 (0.15/0.17), and 3.790(4) Å for Nd5–Nd6 (0.11/0.09). In the major Nd_2 site, Nd atoms also tend to coordinate with fullerene hexagons but are displaced from the center, so that hapticity is better described as η^4.

In both crystal structures, NiOEP molecules show translational disorder over two sites with the major site occupancies of 0.92–0.95 for $Nd_2@I_h$-$C_{80}(CF_3)$ and 0.85 for $Nd_2@D_{5h}$-$C_{80}(CF_3)$ (Figure S12, Supporting Information). Similar phenomenon was described in the NiOEP co-crystals of $Sc_3N@C_{2v}(7854)$-C_{70}[27] and $Tb_2@I_h(7)$-$C_{80}(CF_3)$.[5e] Besides, in both crystals the $Nd_2@C_{80}(CF_3)$ moiety is clamped by two NiOEP molecules (Figure 6), which is a rather rare motif in fullerene·NiOEP co-crystals[5e,28] as fullerenes usually prefer 1:1 complexation with octaethylporphyrin.

Comparison of $Nd_2@C_{80}(CF_3)$ to other $M_2@C_{80}$ di-EMFs with single-electron lanthanide–lanthanide bonds characterized by SC-XRD (Table S3, Supporting Information) shows that the Nd—Nd bond length of 3.78–3.79 Å is very similar to La—La bonds (3.78–3.79 Å),[5b] but shorter than Gd—Gd (3.83 Å),[9a] Tb—Tb (3.84–3.90 Å),[3a,5e] and Dy—Dy bonds (3.89–3.90 Å).[5d,10a] A systematic increase of the M—M bond distance in the lanthanide row despite the lanthanide contraction is caused by the rigid size of the C_{80} fullerene cage and shortening of optimal M—C bond lengths, which inevitably leads to the increase of the M—M distance (see Table S4, Supporting Information, for selected M—C bond lengths from DFT calculations).

2.5. CF$_3$ Addition Sites and Endohedral Positions of Nd$_2$ Dimer

Because of its high symmetry, the I_h-C_{80} cage has only two types of carbons, 20 located on triple-hexagon junctions (THJ) and 60 on pentagon–hexagon–hexagon junctions (PHHJ). Addition of radical groups to THJ carbons is usually strongly energetically unfavorable in comparison to the PHHJ counterparts.[22] Thus, in accordance with the THJ-avoidance rule, the CF$_3$ group in $Nd_2@I_h$-$C_{80}(CF_3)$ is attached to a PHHJ carbon as in the isostructural $Tb_2@I_h$-$C_{80}(CF_3)$.[5e] DFT calculations for different orientations of the Nd_2 dimer inside the I_h-$C_{80}(CF_3)$ moiety revealed the pattern similar to the observed in $M_2@C_{80}(R)$ adducts of heavy lanthanides (R = CF$_3$, CH$_2$Ph).[5c–e] Namely, the Nd_2 dimer tends to avoid the C-sp^3 carbon at the CF$_3$ addition site and adopts positions along the belt of hexagons near the plane, located roughly perpendicular to the C_{80}–CF$_3$ bond (Figure S14, Supporting Information). Several conformers of this sort found in our calculations are isoenergetic within few kJ mol^{-1} (Figure S14, Supporting Information), indicating that the Nd_2 dimer is likely to experience a quasi-2D rotation. The Nd_2 sites in the SC-XRD structure of $Nd_2@I_h$-$C_{80}(CF_3)$ correspond to some of these conformers (Figure 7; Figures S15 and S16, Supporting Information), and their particular positions are determined by interactions with NiOEP molecules since all Nd sites in the experimental structure are found close to Ni—N bonds of nearby porphyrins (Figures S11, S15, and S16, Supporting Information).

As the high symmetry of I_h-C_{80} leaves essentially no alternatives for CF$_3$ addition site in $Nd_2@I_h$-CF$_3$, it cannot be concluded for certain whether the orientation of the Nd_2 dimer in $[Nd_2@I_h$-$C_{80}]^-$ determines which of 60 PHHJ carbons acts as the addition site of the CF$_3$ group, or the CF$_3$ group first adds to a random PHHJ position, and then the Nd_2 dimer adjusts its orientation. The lower symmetry of the D_{5h}-C_{80} cage gives more room for such an analysis. Notably, D_{5h}-C_{80} isomers of lanthanide di-EMFs are less abundant than I_h-C_{80}, and information about their chemical properties is very scarce.[5b,29] $Nd_2@D_{5h}$-$C_{80}(CF_3)$ obtained in this work is only the second example of the di-EMF derivatives with this cage.

D_{5h}-C_{80} has six types of carbon atoms (four PHHJ types and two THJ types), but the endohedral metal dimer will reduce the symmetry and increase the number of non-equivalent carbons. Therefore, we first performed DFT calculations for $[Nd_2@D_{5h}$-$C_{80}]^-$ anion with various orientations of the Nd_2 dimer to find the most preferable metal positions. The structure of the lowest-energy conformer is shown in Figure 1c and 8a, while five other
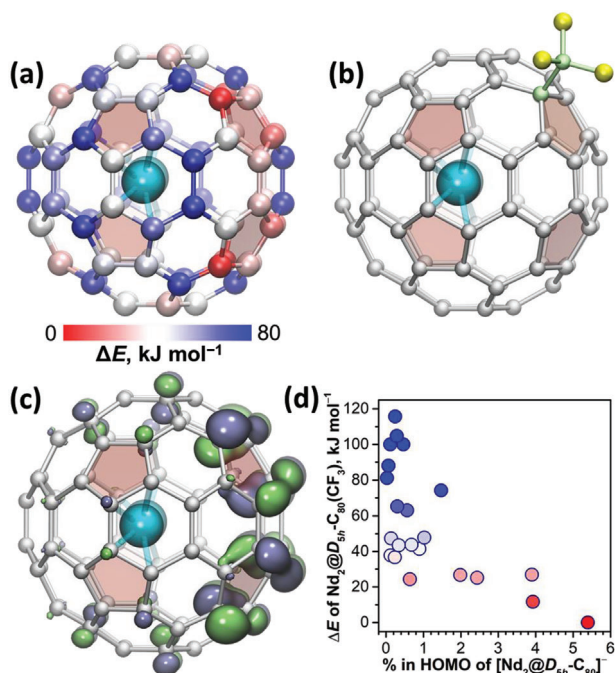
Figure 8. a) $Nd_2@D_{5h}\text{-}C_{80}$ with carbon atoms colored according to the stability of corresponding $Nd_2@C_{80}(CF_3)$ isomers (positions with $\Delta E > 80$ kJ mol^{-1} are all blue). b) The most stable isomer of $Nd_2@D_{5h}\text{-}C_{80}(CF_3)$ according to DFT calculations. c) Isosurface of the α-HOMO of $[Nd_2@D_{5h}\text{-}C_{80}]^-$; note that spin-up ($\alpha$) and spin-down ($\beta$) counterparts of the HOMO are identical (hence only α part is plotted), whereas the singly-occupied Nd—Nd bonding orbital is α-HOMO−1 and has lower energy than the fullerene-based α-HOMO. d) Correlation between contributions of carbons to the α-HOMO of $[Nd_2@D_{5h}\text{-}C_{80}]^-$ and relative energies of corresponding $Nd_2@C_{80}(CF_3)$ isomers.

conformers appeared less stable by 22–57 kJ mol^{-1} (Figure S17, Supporting Information). A similar position of Ce atoms was found earlier in the most stable conformer of $Ce_2@D_{5h}\text{-}C_{80}$.[29,30] Interestingly, despite the C_{2v} point symmetry of this structure, the ^{13}C NMR study of $Ce_2@D_{5h}\text{-}C_{80}$ demonstrated the effective D_{5h} cage symmetry in solution at 280–300 K, proving the rotation of the metal dimer inside the fullerene near room temperature on the NMR timescale.[29]

Having established the most stable structure of $[Nd_2@D_{5h}\text{-}C_{80}]^-$, we optimized all 22 regioisomers of $Nd_2@D_{5h}\text{-}C_{80}(CF_3)$ obtained by addition of a CF_3 group to this conformer (Figure 8a). This survey showed that the isomer corresponding to the experimental SC-XRD structure has the lowest energy (Figure 8b). It has CF_3 group in the same position, to which the radical group was added in $La_2@D_{5h}\text{-}C_{80}(C_3N_3\text{-}Ph_2)$.[5b] The second most stable isomer is at 12 kJ mol^{-1}, and all the others span the relative energy range of 24–120 kJ mol^{-1} (Figure 8a and Figure S18, Supporting Information). To find the rationale for the enhanced stability of the experimental $Nd_2@D_{5h}\text{-}C_{80}(CF_3)$ regioisomer, we analyzed structural and electronic properties of $[Nd_2@D_{5h}\text{-}C_{80}]^-$. Neither atomic charges nor pyramidalization of carbons in pristine $[Nd_2@D_{5h}\text{-}C_{80}]^-$ exhibited discernible correlation with the relative energy of $Nd_2@D_{5h}\text{-}C_{80}(CF_3)$ regioisomers. More revealing appeared the MO analysis, which showed that the most stable regioisomers have CF_3 group on the carbons with the largest

contribution to the HOMO of $[Nd_2@D_{5h}\text{-}C_{80}]^-$ (Figure 8c,d). The same atoms also have the largest spin populations in the pseudo-triplet state of the neutral $Nd_2@D_{5h}\text{-}C_{80}$ (Figure 1c).

Calculations also showed that the CF_3 addition to positions equivalent in the empty $D_{5h}\text{-}C_{80}$ cage, but inequivalent when the metal dimer is considered in $Nd_2@D_{5h}\text{-}C_{80}$, leads to structures with substantially different stability and the relative energy spread of 48 kJ mol^{-1} (Figure S18, Supporting Information). As the Nd_2 dimer did not undergo noticeable rearrangements in the course of optimization, another series of calculations was performed, in which the CF_3 position was fixed to the experimental one, while the orientation of the metal dimer was varied. These calculations localized 11 conformers of $Nd_2@D_{5h}\text{-}C_{80}(CF_3)$ (Figure S19, Supporting Information), twice more than for the bare $[Nd_2@D_{5h}\text{-}C_{80}]^-$ anion. Nonetheless, position of the Nd_2 dimer in the lowest-energy conformer of $Nd_2@D_{5h}\text{-}C_{80}(CF_3)$ (Figure 8b) remained the same as in the most stable conformer of $[Nd_2@D_{5h}\text{-}C_{80}]^-$, whereas other Nd_2 orientations increase the energy by 24–70 kJ mol^{-1}. Thus, rotation of Nd_2 in $Nd_2@D_{5h}\text{-}C_{80}(CF_3)$ is considerably hindered in comparison to $Nd_2@I_h\text{-}C_{80}(CF_3)$. As electrostatic stabilization of metal cations inside negatively charged carbon cages is one of the factors determining stability of metallofullerenes, we also analyzed electrostatic potential (ESP) distribution inside $[D_{5h}\text{-}C_{80}]^{6-}$ and $[D_{5h}\text{-}C_{80}(CF_3)]^{5-}$ (Figure S20, Supporting Information). While ESP distribution in the non-functionalized fullerene is quite uniform and has nearly spherical shape without well-localized minimum, addition of CF_3 group results in considerable inhomogeneity of ESP in $[D_{5h}\text{-}C_{80}(CF_3)]^{5-}$. Importantly, the minimum of ESP in the latter is close to the position of one of Nd atoms in the lowest-energy conformer of $Nd_2@D_{5h}\text{-}C_{80}(CF_3)$.

Comparison of the experimental positions of Nd atoms in the SC-XRD structure of $Nd_2@D_{5h}\text{-}C_{80}(CF_3)$ is complicated by the overlap of two fullerene orientations, which doubles the number of possible orientations for each Nd_2 site and precludes their ascribing to the particular cage orientation solely on the base of SC-XRD data (Figure S21, Supporting Information). Careful analysis augmented with DFT calculations showed that Nd1–Nd2 and Nd5–Nd6 sites correspond to the lowest-energy conformer of $Nd_2@D_{5h}\text{-}C_{80}(CF_3)$ (Figure S21, Supporting Information). The situation is more ambiguous for the Nd3–Nd4 site, but in one of the cage orientations metal atoms are also not strongly displaced from the most stable conformer (Figure 7 and Figure S22, Supporting Information). Based on these findings, we conclude that the Nd_2 dimer in the experimental structure of $Nd_2@D_{5h}\text{-}C_{80}(CF_3)$ is located near the DFT-predicted energy minimum, while the disorder of Nd sites reflects a large-amplitude librational and translational motion of the Nd_2 dimer around its optimal position. Such motions of metal atoms are quite common for metallofullerenes because, when metal atoms are encapsulated inside the fullerene cage, their translational degrees of freedom transform into vibrations with librational and translational character. Lateral vibrational modes, in which metal atoms are displaced parallel to the fullerene surface, occur at low frequencies (<100 cm^{-1}), in part because metal atoms are heavy, and in part because potential energy surface for such displacements is often rather flat. The low frequencies imply the ease of thermal excitation and the large amplitude of such motions.
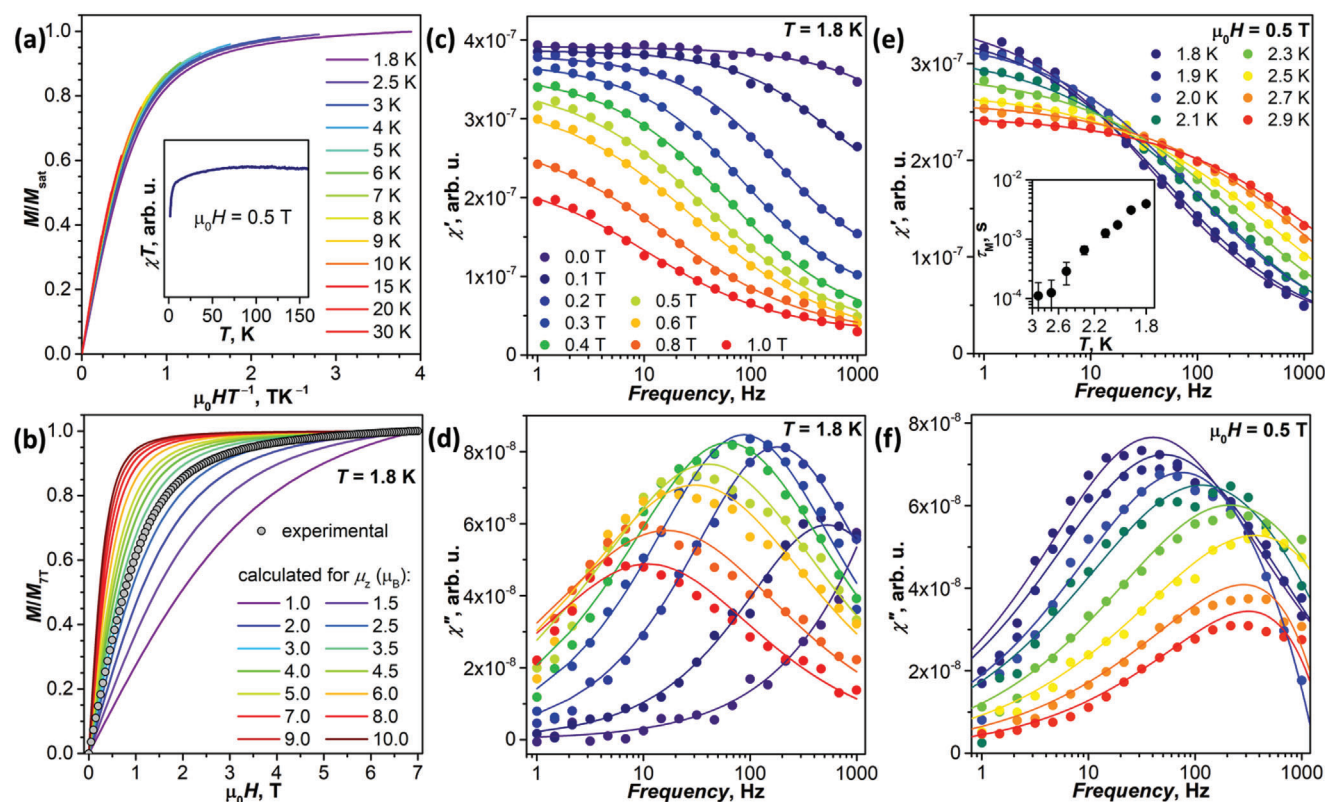
**ADVANCED
SCIENCE NEWS**

www.advancedsciencenews.com

**ADVANCED
SCIENCE**
Open Access

www.advancedscience.com

Figure 9. Magnetic properties of $Nd_2@I_h-C_{80}(CF_3)$. a) MT^{-1} product at different temperatures, the inset shows χT curve measured in the field of 0.5 T. b) Calculated normalized magnetization curves for axially-anisotropic molecules with different μ_z compared to the normalized experimental magnetization curve of $Nd_2@I_h-C_{80}(CF_3)$. c,d) In-phase (χ') and out-of-phase (χ'') magnetic susceptibility measured in different fields at 1.8 K. e,f) In-phase (χ') and out-of-phase (χ'') magnetic susceptibility measured at different temperatures in the field of 0.5 T; the inset in (e) shows the temperature dependence of relaxation times.

Extended DFT calculations described in this section prove that the experimental structure of $Nd_2@D_{5h}-C_{80}(CF_3)$ corresponds to the most thermodynamically stable isomer. However, it would be too hasty to conclude that the electrophilic CF_3 addition to $[M_2@C_{80}]^-$ proceeds under thermodynamic control. The latter implies that CF_3 groups bonded to a fullerene can rearrange on its surface via detachment/attachment steps until the most thermodynamically favorable position is achieved. But CF_3 derivatives of fullerenes are extremely thermally stable,[22] and detachment of CF_3 groups occurs only at high temperatures ($T >$ 300°C).[28i,31] It is therefore very unlikely that a CF_3 group, once it formed a bond with a certain carbon atom of $Nd_2@C_{80}$, can rearrange to a different site at room temperature in solution. The correlation between the isomer stability and the shape of the HOMO suggests that thermodynamically favorable products of the electrophilic trifluoromethylation of $[M_2@C_{80}]^-$ and presumably other EMF anions are also favorable kinetically. The spatial distribution of the HOMO, in its turn, is strongly related to the position of the metal dimer (Figure 8c), and it would be reasonable to conclude that the CF_3 addition site is to a large extent controlled by the metal dimer. Even though the latter can often rotate inside a fullerene, its momentary position at the time of the attack will determine where the HOMO is localized and which carbons will act as CF_3 addition sites.

2.6. Magnetic Properties of $Nd_2@I_h-C_{80}(CF_3)$

Single-electron metal–metal bonds lead to strong exchange interactions in endohedral lanthanide dimers, which earlier resulted in dramatic improvement of the single-molecule magnetism (SMM) in Dy_2 and Tb_2 compounds.[5,10,11] To find if similar phenomena take place in Nd_2, we studied magnetic properties of $Nd_2@I_h-C_{80}(CF_3)$ with SQUID magnetometry. M versus HT^{-1} plots do not superimpose, indicating magnetic anisotropy and/or thermally accessible excited magnetic states (**Figure 9a**). Unfortunately, the low available amount of the sample (≈2.5 mg) and its small magnetization prevent accurate determination of the magnetic moment from the saturated magnetization, and we had to rely on the shapes of magnetization curves for a conservative estimation. Figure 9b compares normalized magnetization curves (M/M_{7T}) simulated for powder samples of axially anisotropic magnetic moments with μ_z ranging from 1 to 10 μ_B. If, similar to Tb and Dy analogs,[5] Nd ions in $Nd_2@I_h-C_{80}(CF_3)$ were having axial single-ion magnetic anisotropy with the largest J_z projection of 9/2 and ferromagnetic coupling of collinear Nd and unpaired electron magnetic moments, the total moment of the molecule would be 7.545 μ_B. However, experimental magnetization curve of $Nd_2@I_h-C_{80}(CF_3)$ closely follows the simulated one for μ_z of only 3 μ_B (Figure 9b). Several factors may contribute to such a small magnetic moment, including a weak

exchange coupling, a small single-ion anisotropy of Nd ions, a non-collinear arrangement of the moments, or a combination of several of these factors. Deeper understanding of how magnetic moments of Nd ions interact in $Nd_2@I_h\text{-}C_{80}(CF_3)$ will require advanced computational ab initio modeling, which is beyond the scope of this work.

$Nd_2@I_h\text{-}C_{80}(CF_3)$ did not show magnetic hysteresis down to 1.8 K, and we performed AC measurement to understand if the relaxation of magnetization may still happen on a sub-second time scale. At 1.8 K in zero static magnetic field, only a tail of the χ'' peak could be detected (Figure 9c,d), which means that the relaxation is too fast in the frequency range of 1000 Hz. However, an increase of the static field decelerated the process and shifted the χ'' peak to lower frequencies (Figure 9d). The temperature dependence measured in the static field of 0.5 T revealed a fast increase of the relaxation rate with temperature, giving the upper temperature limit of only 3 K (Figure 9e,f). Thus, $Nd_2@I_h\text{-}C_{80}(CF_3)$ exhibits properties of a weak field-induced SMM akin to many other Nd-SMMs,[32] but the very limited temperature range does not allow us to analyze its relaxation mechanisms.

3. Conclusions

The ability of fullerenes to encapsulate metal dimers with M–M bonds is utilized to obtain the first instance of covalent Nd–Nd bond. First, we performed a systematic DFT study of lanthanide $M_2@C_{80}$ with different lanthanides and found that $Nd_2@C_{80}$ is on the border between two types of di-EMFs. One type forms $M_2@C_{80}$ molecules with pseudo-singlet ground state without M–M bonding, whereas another type features a single-electron M–M bond in the pseudo-triplet ground state. The synthesis of Nd EMFs with subsequent DMF extraction and reaction of the anionic extract with electrophilic "CF_3^+" reagent allowed isolation of two $Nd_2@C_{80}(CF_3)$ adducts. Crystallographic analysis determined that these compounds are based on $I_h\text{-}C_{80}$ and $D_{5h}\text{-}C_{80}$ cage isomers and both feature a single-electron Nd–Nd bond with the length of ≈ 3.8 Å. Relatively low symmetry of $Nd_2@D_{5h}\text{-}C_{80}$ cage enabled analysis of the factors affecting regioselectivity of electrophilic trifluoromethylation of EMF anions and the mutual influence of CF_3 and metal dimer. The influence of the Nd–Nd bond on magnetization dynamics was studied by SQUID magnetometry, which revealed that $Nd_2@I_h\text{-}C_{80}(CF_3)$ is a weak SMM. Its slow relaxation of magnetization could be detectable only below 3 K in the presence of magnetic field, while no magnetic hysteresis was observed. This behavior is quite different from Dy and Tb dimetallofullerenes with single-electron metal–metal bond, showing that M–M bonds in light lanthanides may lead to different properties and require further studies.

Supporting Information

Supporting Information is available from the Wiley Online Library or from the author.

Conflict of Interest

The authors declare no conflict of interest.

Data Availability Statement

The data that support the findings of this study are available in the supplementary material of this article.

[1] a) A. A. Popov, S. Yang, L. Dunsch, *Chem. Rev.* **2013**, *113*, 5989; b) S. Yang, T. Wei, F. Jin, *Chem. Soc. Rev.* **2017**, *46*, 5005; c) W. Cai, C. H. Chen, N. Chen, L. Echegoyen, *Acc. Chem. Res.* **2019**, *52*, 1824; d) W. Shen, L. Bao, X. Lu, *Chin. J. Chem.* **2022**, *40*, 275; e) J. Zhuang, R. Morales-Martínez, J. Zhang, Y. Wang, Y. R. Yao, C. Pei, A. Rodríguez-Fortea, S. Wang, L. Echegoyen, C. De Graaf, J. M. Poblet, N. Chen, *Nat. Commun.* **2021**, *12*, 2372; f) A. Moreno-Vicente, Y. Roselló, N. Chen, L. Echegoyen, P. W. Dunk, A. Rodríguez-Fortea, C. De Graaf, J. M. Poblet, *J. Am. Chem. Soc.* **2023**, *145*, 6710; g) W. Xiang, Z. Hu, J. Xin, H. Jin, Z. Jiang, X. Han, M. Chen, Y. R. Yao, S. Yang, *J. Am. Chem. Soc.* **2023**, *145*, 22599.

[2] a) A. A. Popov, S. M. Avdoshenko, A. M. Pendás, L. Dunsch, *Chem. Commun.* **2012**, *48*, 8031; b) L. Bao, P. Peng, X. Lu, *Acc. Chem. Res.* **2018**, *51*, 810; c) F. Liu, L. Spree, D. S. Krylov, G. Velkos, S. M. Avdoshenko, A. A. Popov, *Acc. Chem. Res.* **2019**, *52*, 2981.

[3] a) T. Zuo, L. Xu, C. M. Beavers, M. M. Olmstead, W. Fu, T. D. Crawford, A. L. Balch, H. C. Dorn, *J. Am. Chem. Soc.* **2008**, *130*, 12992; b) W. Fu, J. Zhang, T. Fuhrer, H. Champion, K. Furukawa, T. Kato, J. E. Mahaney, B. G. Burke, K. A. Williams, K. Walker, C. Dixon, J. Ge, C. Shu, K. Harich, H. C. Dorn, *J. Am. Chem. Soc.* **2011**, *133*, 9741.

[4] a) T. Yang, X. Zhao, E. Osawa, *Chem. - Eur. J.* **2011**, *17*, 10230; b) N. A. Samoylova, S. M. Avdoshenko, D. S. Krylov, H. R. Thompson, A. C. Kirkhorn, M. Rosenkranz, S. Schiemenz, F. Ziegs, A. U. B. Wolter, S. Yang, S. Stevenson, A. A. Popov, *Nanoscale* **2017**, *9*, 7977; c) W. Shen, L. Bao, Y. Wu, C. Pan, S. Zhao, H. Fang, Y. Xie, P. Jin, P. Peng, F. F. Li, X. Lu, *J. Am. Chem. Soc.* **2017**, *139*, 9979; d) X. Lu, S. Hu, W. Shen, G. Duan, L. Yang, P. Jin, Y. Xie, T. Akasaka, *Chem. - Eur. J.* **2019**, *25*, 11538; e) C. Pan, W. Shen, L. Yang, L. Bao, Z. Wei, P. Jin, H. Fang, Y. Xie, T. Akasaka, X. Lu, *Chem. Sci.* **2019**, *10*, 4707.

[5] a) L. Bao, M. Chen, C. Pan, T. Yamaguchi, T. Kato, M. M. Olmstead, A. L. Balch, T. Akasaka, X. Lu, *Angew. Chem., Int. Ed.* **2016**, *55*, 4242; b) M. Yamada, H. Kurihara, M. Suzuki, M. Saito, Z. Slanina, F. Uhlik, T. Aizawa, T. Kato, M. M. Olmstead, A. L. Balch, Y. Maeda, S. Nagase, X. Lu, T. Akasaka, *J. Am. Chem. Soc.* **2015**, *137*, 232; c) F. Liu, G.

Velkos, D. S. Krylov, L. Spree, M. Zalibera, R. Ray, N. A. Samoylova, C. H. Chen, M. Rosenkranz, S. Schiemenz, F. Ziegs, K. Nenkov, A. Kostanyan, T. Greber, A. U. B. Wolter, M. Richter, B. Büchner, S. M. Avdoshenko, A. A. Popov, *Nat. Commun.* **2019**, *10*, 571; d) F. Liu, D. S. Krylov, L. Spree, S. M. Avdoshenko, N. A. Samoylova, M. Rosenkranz, A. Kostanyan, T. Greber, A. U. B. Wolter, B. Büchner, A. A. Popov, *Nat. Commun.* **2017**, *8*, 16098; e) Y. Wang, G. Velkos, N. J. Israel, M. Rosenkranz, B. Büchner, F. Liu, A. A. Popov, *J. Am. Chem. Soc.* **2021**, *143*, 18139; f) Z. Wang, R. Kitaura, H. Shinohara, *J. Phys. Chem. C* **2014**, *118*, 13953.

[6] a) A. A. Popov, L. Zhang, L. Dunsch, *ACS Nano* **2010**, *4*, 795; b) Y.-J. Guo, H. Zheng, T. Yang, S. Nagase, X. Zhao, *Inorg. Chem.* **2015**, *54*, 8066; c) Y. Jiang, Z. Li, Y. Wu, Z. Wang, *Inorg. Chem. Front.* **2022**, *9*, 2173.

[7] a) F. Jin, J. Xin, R. Guan, X. M. Xie, M. Chen, Q. Zhang, A. A. Popov, S.-Y. Xie, S. Yang, *Chem. Sci.* **2021**, *12*, 6890; b) S. Hu, P. Zhao, B. Li, P. Yu, L. Yang, M. Ehara, P. Jin, T. Akasaka, X. Lu, *Inorg. Chem.* **2022**, *61*, 11277.

[8] M. Nie, L. Yang, C. Zhao, H. Meng, L. Feng, P. Jin, C. Wang, T. Wang, *Nanoscale* **2019**, *11*, 18612.

[9] a) Z. Hu, B.-W. Dong, Z. Liu, J. J. Liu, J. Su, C. Yu, J. Xiong, D.-E. Shi, Y. Wang, B.-W. Wang, A. Ardavan, Z. Shi, S.-D. Jiang, S. Gao, *J. Am. Chem. Soc.* **2018**, *140*, 1123; b) G. Velkos, D. S. Krylov, K. Kirkpatrick, X. Liu, L. Spree, A. U. B. Wolter, B. Büchner, H. C. Dorn, A. A. Popov, *Chem. Commun.* **2018**, *54*, 2902; c) F. Cimpoesu, B. Frecus, C. I. Oprea, H. Ramanantoanina, W. Urland, C. Daul, *Mol. Phys.* **2015**, *113*, 1712; d) G. Rajaraman, M. K. Singh, N. Yadav, *Chem. Commun.* **2015**, *51*, 17732.

[10] a) Y. Wang, J. Xiong, J. Su, Z. Hu, F. Ma, R. Sun, X. Tan, H. L. Sun, B.-W. Wang, Z. Shi, S. Gao, *Nanoscale* **2020**, *12*, 11130; b) G. Velkos, D. S. Krylov, K. Kirkpatrick, L. Spree, V. Dubrovin, B. Büchner, S. M. Avdoshenko, V. Bezmelnitsyn, S. Davis, P. Faust, J. Duchamp, H. C. Dorn, A. A. Popov, *Angew. Chem., Int. Ed.* **2019**, *58*, 5891; c) L. Spree, F. Liu, V. Neu, M. Rosenkranz, G. Velkos, Y. Wang, S. Schiemenz, J. Dreiser, P. Gargiani, M. Valvidares, C. H. Chen, B. Büchner, S. M. Avdoshenko, A. A. Popov, *Adv. Funct. Mater.* **2021**, *31*, 2105516; d) F. Paschke, T. Birk, V. Enenkel, F. Liu, V. Romankov, J. Dreiser, A. A. Popov, M. Fonin, *Adv. Mater.* **2021**, *33*, 2102844.

[11] a) C. A. Gould, K. R. Mcclain, D. Reta, J. G. C. Kragskow, D. A. Marchiori, E. Lachman, E. S. Choi, J. G. Analytis, R. D. Britt, N. F. Chilton, B. G. Harvey, J. R. Long, *Science* **2022**, *375*, 198; b) K. R. Mcclain, H. Kwon, K. Chakarawet, R. Nabi, J. G. C. Kragskow, N. F. Chilton, R. D. Britt, J. R. Long, B. G. Harvey, *J. Am. Chem. Soc.* **2023**, *145*, 8996.

[12] a) A. Velloth, Y. Imamura, T. Kodama, M. Hada, *J. Phys. Chem. C* **2017**, *121*, 18169; b) A. Velloth, Y. Imamura, T. Kodama, M. Hada, *J. Phys. Chem. C* **2017**, *121*, 27700.

[13] a) H. Yang, H. Jin, B. Hong, Z. Liu, C. M. Beavers, H. Zhen, Z. Wang, B. Q. Mercado, M. M. Olmstead, A. L. Balch, *J. Am. Chem. Soc.* **2011**, *133*, 16911; b) B. Q. Mercado, A. Jiang, H. Yang, Z. Wang, H. Jin, Z. Liu, M. M. Olmstead, A. L. Balch, *Angew. Chem., Int. Ed.* **2009**, *48*, 9114.

[14] J. Ding, S. Yang, *J. Am. Chem. Soc.* **1996**, *118*, 11254.

[15] a) Y.-L. Zhao, H. T. Tu, Y.-F. Lian, *RSC Adv.* **2016**, *6*, 115113; b) R. J. Nicholls, K. Sader, J. H. Warner, S. R. Plant, K. Porfyrakis, P. D. Nellist, G. A. D. Briggs, D. J. H. Cockayne, *ACS Nano* **2010**, *4*, 3943.

[16] a) Y. Zhang, R. Guan, M. Chen, Y. Shen, Q. Pan, Y. Lian, S. Yang, *Inorg. Chem.* **2021**, *6*, 1462; b) J. Ding, N. Lin, L.-T. Weng, N. Cue, S. Yang, *Chem. Phys. Lett.* **1996**, *261*, 92.

[17] a) J. Ding, S. Yang, *Chem. Mater.* **1996**, *8*, 2824; b) E. E. Laukhina, V. P. Bubnov, Y. I. Estrin, Y. A. Golod, M. A. Khodorkovskii, V. K. Koltover, E. B. Yagubskii, *J. Mater. Chem.* **1998**, *8*, 893.

[18] I. E. Kareev, V. P. Bubnov, E. E. Laukhina, A. F. Dodonov, V. I. Kozlovski, E. B. Yagubskii, *Fullerenes, Nanotubes Carbon Nanostruct.* **2004**, *12*, 65.

[19] D. Sun, H. Huang, S. Yang, Z. Liu, S. Liu, *Chem. Mater.* **1999**, *11*, 374.

[20] T. Tsuchiya, T. Wakahara, Y. Lian, Y. Maeda, T. Akasaka, N. Kato, N. Mizorogi, S. Nagase, *J. Phys. Chem. B* **2006**, *110*, 22517.

[21] T. Umemoto, B. Zhang, T. Zhu, X. Zhou, P. Zhang, S. Hu, Y. Li, *J. Org. Chem.* **2017**, *82*, 7708.

[22] O. V. Boltalina, A. A. Popov, I. V. Kuvychko, N. B. Shustova, S. H. Strauss, *Chem. Rev.* **2015**, *115*, 1051.

[23] H. Shimotani, T. Ito, Y. Iwasa, A. Taninaka, H. Shinohara, E. Nishibori, M. Takata, M. Sakata, *J. Am. Chem. Soc.* **2004**, *126*, 364.

[24] U. Mueller, R. Förster, M. Hellmig, F. U. Huschmann, A. Kastner, P. Malecki, S. Pühringer, M. Röwer, K. Sparta, M. Steffien, M. Ühlein, P. Wilk, M. S. Weiss, *Eur. Phys. J. Plus* **2015**, *130*, 141.

[25] a) W. Kabsch, *Acta Crystallogr., Sect. D: Struct. Biol.* **2010**, *66*, 125; b) K. M. Sparta, M. Krug, U. Heinemann, U. Mueller, M. S. Weiss, *J. Appl. Crystallogr.* **2016**, *49*, 1085.

[26] G. M. Sheldrick, *Acta Crystallogr. C* **2015**, *71*, 3.

[27] Y. Hao, Y. Wang, V. Dubrovin, S. M. Avdoshenko, A. A. Popov, F. Liu, *J. Am. Chem. Soc.* **2021**, *143*, 612.

[28] a) Y. Zhang, K. B. Ghiassi, Q. Deng, N. A. Samoylova, M. M. Olmstead, A. L. Balch, A. A. Popov, *Angew. Chem., Int. Ed.* **2015**, *52*, 495; b) Y. Sado, S. Aoyagi, R. Kitaura, Y. Miyata, E. Nishibori, H. Sawa, K. Sugimoto, H. Shinohara, *J. Phys. Chem. C* **2013**, *117*, 6437; c) H. Kurihara, X. Lu, Y. Iiduka, H. Nikawa, M. Hachiya, N. Mizorogi, Z. Slanina, T. Tsuchiya, S. Nagase, T. Akasaka, *Inorg. Chem.* **2012**, *51*, 746; d) Y. Che, H. Yang, Z. Wang, H. Jin, Z. Liu, C. Lu, T. Zuo, H. C. Dorn, C. M. Beavers, M. M. Olmstead, A. L. Balch, *Inorg. Chem.* **2009**, *48*, 6004; e) C. M. Beavers, H. Jin, H. Yang, Z. Wang, X. Wang, H. Ge, Z. Liu, B. Q. Mercado, M. M. Olmstead, A. L. Balch, *J. Am. Chem. Soc.* **2011**, *133*, 15338; f) B. Q. Mercado, A. Jiang, H. Yang, Z. Wang, H. Jin, Z. Liu, M. M. Olmstead, A. L. Balch, *Angew. Chem., Int. Ed.* **2009**, *48*, 9114; g) C. Pan, L. Bao, X. Yu, H. Fang, Y. Xie, T. Akasaka, X. Lu, *ACS Nano* **2018**, *12*, 2065; h) A. Nakagawa, S. Aoyagi, K. Ishino, M. Nishino, J. Rio, C. Ewels, H. Shinohara, *R. Soc. Open Sci.* **2018**, *5*, 181015; i) O. O. Semivrazhskaya, A. V. Rybalchenko, M. P. Kosaya, N. S. Lukonina, O. N. Mazaleva, I. N. Ioffe, S. I. Troyanov, N. B. Tamm, A. A. Goryunkov, *Electrochim. Acta* **2017**, *255*, 472; j) L. M. Baldauf, J. C. Fettinger, M. M. Olmstead, K. B. Ghiassi, A. L. Balch, *Cryst. Growth Des.* **2023**, *23*, 915; k) M. Roy, M. M. Olmstead, A. L. Balch, *Cryst. Growth Des.* **2019**, *19*, 6743.

[29] M. Yamada, N. Mizorogi, T. Tsuchiya, T. Akasaka, S. Nagase, *Chem. - Eur. J.* **2009**, *15*, 9486.

[30] L. Feng, M. Suzuki, N. Mizorogi, X. Lu, M. Yamada, T. Akasaka, S. Nagase, *Chem. - Eur. J.* **2013**, *19*, 988.

[31] a) N. M. Belov, M. G. Apenova, A. V. Rybalchenko, E. V. Borkovskaya, N. S. Lukonina, A. A. Goryunkov, I. N. Ioffe, S. I. Troyanov, L. N. Sidorov, *Chem. - Eur. J.* **2014**, *20*, 1126; b) D. V. Ignat'eva, T. Mutig, A. A. Goryunkov, N. B. Tamm, E. Kemnitz, S. I. Troyanov, L. N. Sidorov, *Russ. Chem. Bull.* **2009**, *58*, 1146; c) T. Mutig, E. Kemnitz, S. I. Troyanov, *Mendeleev Commun.* **2009**, *19*, 30.

[32] a) F. Pointillart, O. Cador, B. Le Guennic, L. Ouahab, *Coord. Chem. Rev.* **2017**, *346*, 150; b) A. Borah, R. Murugavel, *Coord. Chem. Rev.* **2022**, *453*, 214288.

2305190 (10 of 10)